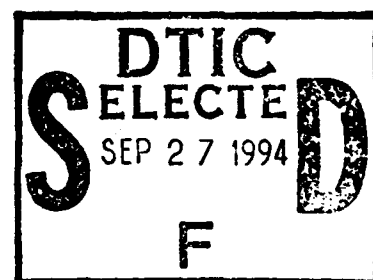# A TRIDENT SCHOLAR
PROJECT REPORT

NO.212

AD-A284 857

MODELING THE DIURNALLY PRECESSING JOVIAN
MAGNETOSPHERIC FIELD

UNITED STATES NAVAL ACADEMY
ANNAPOLIS, MARYLAND

94-30774

MODELING THE DIURNALLY PRECESSING JOVIAN MAGNETOSPHERIC FIELD

by
Midshipman Todd D. Bode, Class of 1994
U.S. Naval Academy
Annapolis, Maryland

Irene M. Engle

Adviser: Associate Professor Irene M. Engle
Physics Department

Accepted for Trident Scholar Committee

Francis D Correll

Chair

19 May 1994

Date

DTIC QUALITY INSPECTED 3

USNA-1531-2

REPORT DOCUMENTATION PAGE

Public reporting burden for this collection of information is estimated to average 1 hour of response, including the time for reviewing instructions, searching existing data sources, gathering and maintaining the data needed, and completing and reviewing the collection of information. Send comments regarding this burden estimate or any other aspect of this collection of information, including suggestions for reducing this burden, to Washington Headquarters Services, Directorate for Information Operations and Reports, 1215 Jefferson Davis Highway, Suite 1204, Arlington, VA 22202-4302, and to the Office of Management and Budget, Paperwork Reduction Project (0704-0188), Washington DC 20503.

1. AGENCY USE ONLY (Leave blank)	2. REPORT DATE 19 May 1994	3. REPORT TYPE AND DATES COVERED

4. TITLE AND SUBTITLE Modeling the diurnally precessing Jovian magnetospheric field

5. FUNDING NUMBERS

6. AUTHOR(S)

Todd D. Bode

7. PERFORMING ORGANIZATIONS NAME(S) AND ADDRESS(ES)

U.S. Naval Academy, Annapolis, MD

8. PERFORMING ORGANIZATION REPORT NUMBER USNA
Trident Scholar project report; no. 212 (1994)

9. SPONSORING/MONITORING AGENCY NAME(S) AND ADDRESS(ES)

10. SPONSORING/MONITORING AGENCY REPORT NUMBER

11. SUPPLEMENTARY NOTES

Accepted by the U.S. Trident Scholar Committee

12a. DISTRIBUTION/AVAILABILITY STATEMENT

This document has been approved for public release; its distribution is UNLIMITED.

12b. DISTRIBUTION CODE

13. ABSTRACT (Maximum 200 words) A functional representation of the magnetic field contribution of the solar-wind-driven electric currents on the magnetopause of Jupiter is presented. The representation accounts for the precession of the magnetic axis and the consequential diurnal variation of the shape of the magnetopause. Existing models of the two interior field sources (planetary dipole and currents of trapped plasma) were incorporated into a set of eight three-dimensional static models. Each model assumed a 10^0 tilt of the magnetic axis with respect to Jupiter's rotation axis. This set includes representations published [Engle, 1992b] for a tilt toward ($\alpha = 0^0$) and away from ($\alpha = 180^0$) the Sun in the noon-midnight meridian plane, as well as six complementary analogous models for azimuthal angles of 45^0, 90^0, 135^0, 225^0, 270^0, and 315^0. The representations were connected by replacing expansion coefficients with continuous functions which replicated each of the eight original static models and interpolated between them. The result is a time-dependent functional representation of the magnetic potential of the magnetopause surface currents in terms of an expansion in associated Legendre functions. This model yields predicted magnetic field components for any location within the magnetosphere as Jupiter's magnetic axis precesses during the course of a Jovian day ($9^h\ 55^m\ 41^s$).

14. SUBJECT TERMS Jupiter, modeling, planetary, solar wind, Voyager

15. NUMBER OF PAGES

16. PRICE CODE

17. SECURITY CLASSIFICATION OF REPORT	18. SECURITY CLASSIFICATION OF THIS PAGE	19. SECURITY CLASSIFICATION OF ABSTRACT	20. LIMITATION OF ABSTRACT
UNCLASSIFIED	UNCLASSIFIED	UNCLASSIFIED	UNCLASSIFIED

DTIC QUALITY INSPECTED 3

Table of Contents

Abstract

A functional representation of the magnetic field contribution of the solar-wind-driven electric currents on the magnetopause of Jupiter is presented. The representation accounts for the precession of the magnetic axis and the consequential diurnal variation of the shape of the magnetopause. Existing models of the two interior field sources (planetary dipole and currents of trapped plasma) were incorporated into a set of eight three-dimensional static models. Each model assumed a 10° tilt of the magnetic axis with respect to Jupiter's rotation axis. This set includes representations published [*Engle*, 1992*b*] for a tilt toward ($\alpha = 0^o$) and away from ($\alpha = 180^o$) the Sun in the noon-midnight meridian plane, as well as six complementary analogous models for azimuthal angles of 45°, 90°, 135°, 225°, 270°, and 315°. The representations were connected by replacing expansion coefficients with continuous functions which replicated each of the eight original static models and interpolated between them. The result is a time-dependent functional representation of the magnetic potential of the magnetopause surface currents in terms of an expansion in associated Legendre functions. This model yields predicted magnetic field components for any location within the magnetosphere as Jupiter's magnetic axis precesses during the course of a Jovian day (9^h 55^m 41^s).

Keywords

I.   Introduction

In December 1973, on board the Pioneer 10 spacecraft, high-field triaxial fluxgate magnetometers provided the first instantaneous vector measurements of the net magnetospheric field of the planet Jupiter. Without further processing on board the spacecraft, the digitized measurements were sent directly to ground, where raw position and magnetic field data were translated into a Jupiter-centered rectangular coordinate system. Analysis of the field data proved Jupiter's magnetospheric field to be significantly different than had been anticipated [*Smith et al.*, 1974]. An extrapolation based upon a detailed knowledge of the Earth's magnetosphere was consistent with the intrinsic planetary field of Jupiter. Pioneer and later Voyager observations suggested a dipole with dipole moment of about 420,000 nT-R_J^3, where R_J is the Jovian planetary radius, 71433.6 km (Figure 1).

Figure 1.   Dipole approximation of the intrinsic planetary magnetic field of Jupiter. The magnetic axis is tilted 10° away from the rotation axis toward the Sun.
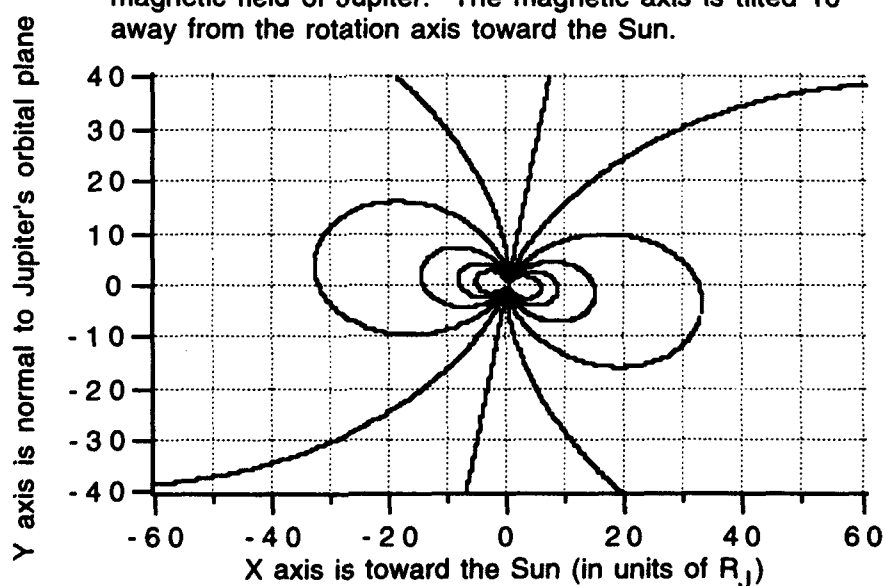
However, the magnetosphere was much larger than had been predicted, and there was an appreciable, co-rotating current sheet located in and near the magnetic equatorial plane. This current sheet was in the form of a plasma, a gas consisting of an equal number of electrons and positive charges. This current sheet extended from about 5 R_J (the orbit of the moon Io) to nearly 100 R_J at the time of the Pioneer encounters. Greater solar wind pressure and/or reduced trapped-plasma pressure during the later Voyager spacecraft encounters led to a more compressed magnetosphere and an observed current sheet extending only 60 R_J from the planet [*Ness et al.*, 1979]. In each case the current sheet increased the net magnetic field. The intrinsic planetary dipole and the currents of charged particles trapped near the planet constitute the two interior field sources.

Figure 2. Jovian model magnetic field due to the Voyager-observed interior field sources. The magnetic axis is tilted 10° from the planet's rotation axis toward the sun.
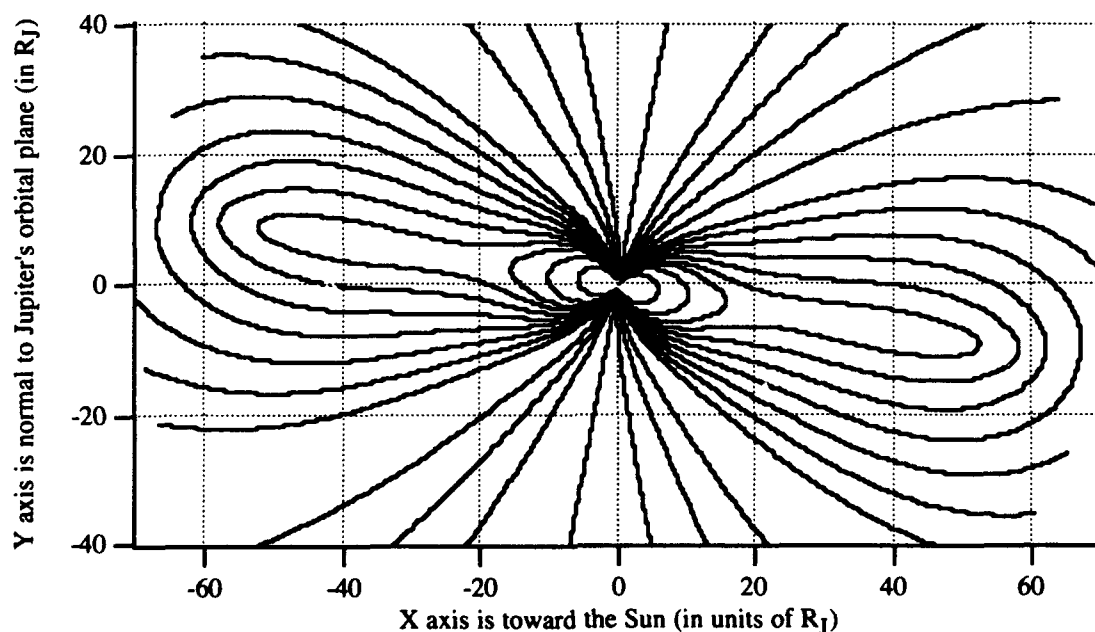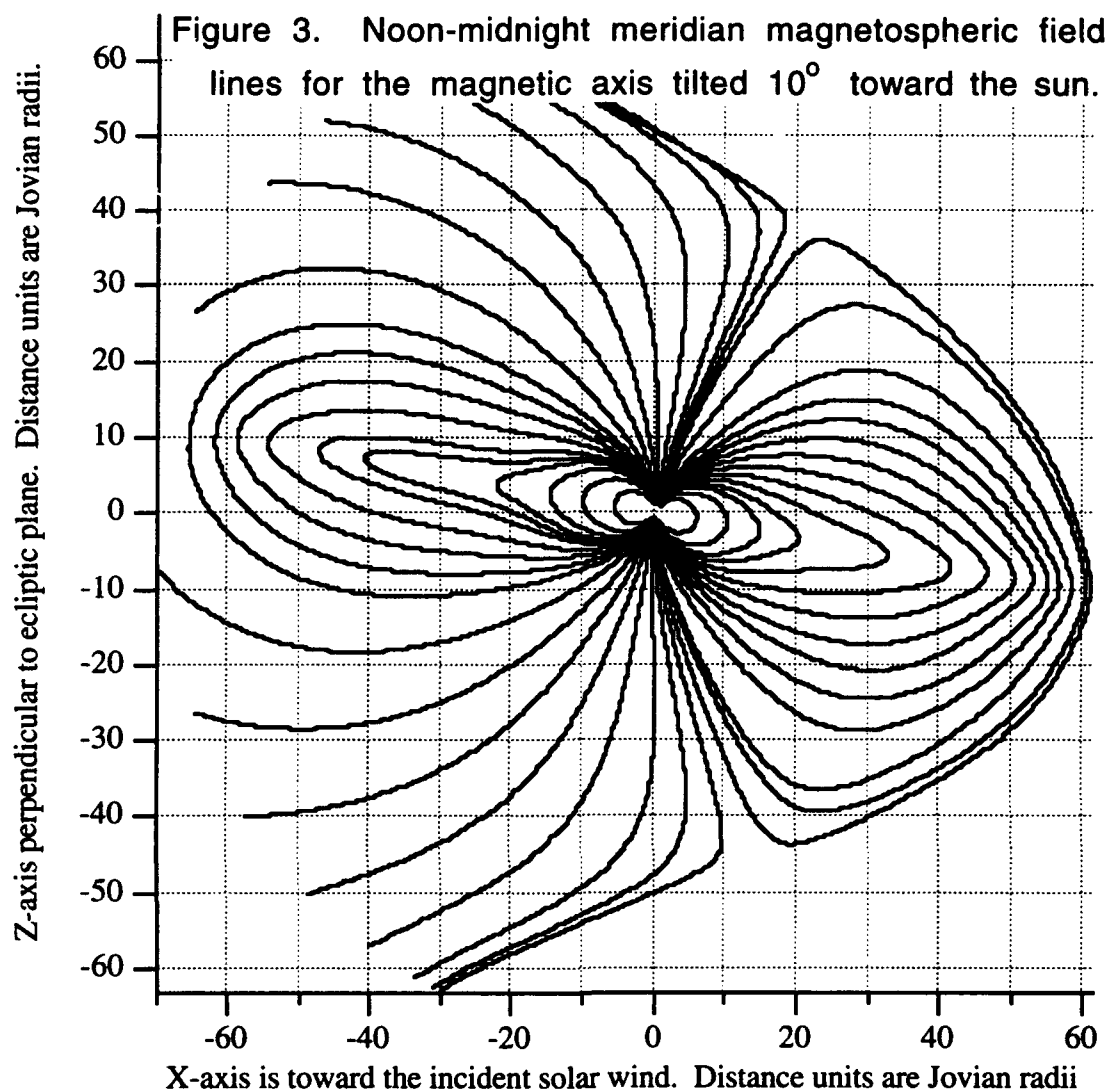
Figure 2 displays the magnetic field due to these interior sources.

The outer limit of Jupiter's magnetosphere is defined by the magnetopause, a literal magnetic field boundary. Only a weak interplanetary magnetic field exists outside of this boundary. Located where the incoming solar wind is deflected by the interior magnetic field, the magnetopause is sensitive to both the intensity of the solar wind and to the specifics of the interior field sources. The solar wind is a stream of charged particles, mostly protons and electrons, which flows from the sun. This high-speed plasma, interacting with the interior field, generates currents on the magnetopause which enhance the field intensity interior to this boundary but cancel the field outside of the region. On the planet's solar side, the magnetosphere is well-defined by the magnetopause, but in the anti-solar direction this region extends millions of kilometers beyond the radius of the planet.

These three sources--the intrinsic planetary dipole approximation, the co-rotating current sheet, and the magnetopause surface currents--describe the large-scale magnetosphere of Jupiter. The net field due to all three primary field sources is displayed in Figure 3.

Figure 3. Noon-midnight meridian magnetospheric field lines for the magnetic axis tilted 10° toward the sun.

II. Preliminary Models

Magnetometer measurements from four spacecraft flybys, each along single line trajectories near Jupiter's orbital plane, have provided the foundation for several global, three-dimensional static models of the Jovian magnetospheric field. There is no unique way to model the observed field. Each successive model attempts to more completely and more accurately represent the magnetosphere region by incorporating the effects of additional physical phenomena

and/or the conclusions of more recent and reliable investigations. Work by a number of investigators, including *Barish and Smith* [1975], *Beard and Jackson* [1976], and references cited by them, led to a Jovian magnetosphere model which included the effects of the solar wind interaction with interior sources corresponding to Pioneer 10 observations [*Engle and Beard*, 1980]. Subsequent Voyager observations led to alternate models. *Connerney et al.* recalculated the planetary dipole [1982] and presented a co-rotating current sheet model with an azimuthal component parallel to the magnetic equator [1981]. *Engle* [1992*a*] used these interior sources to develop an idealized "no tilt" model which incorporated the effects of the solar wind. A subsequent work [*Engle*, 1992*b*] included the effects of the tilt of the magnetic axis away from the normal to the incident solar wind.

III.   Modeling the Magnetopause Surface Currents

The incident solar wind plasma contains, in each unit of volume, approximately equal numbers of positive and negative charges traveling with the same average velocity. Each particle, upon crossing the magnetopause and entering a region of magnetic field, experiences a magnetic force described by

$$\vec{F} = q\,\vec{v} \times \vec{B}, \tag{1}$$

where q is the electric charge on the particle, $\vec{v}$ is the particle's velocity, and $\vec{B}$ is the local magnetic field. The response of charged particles to this force is a deflection of positive charges in one

direction and negative charges in the opposite direction. The net effect of this interaction is that surface current elements form on the magnetopause boundary. The incident neutral particle flux, having no net current associated with the motion of its particles, has the motion of its constituents reordered in such a way as to produce a net current in the direction of the deflection of the positive charges. The magnitude of the net current is twice the magnitude of the current associated with the positive charges alone. Associated with every current is a related magnetic field, as described by the Biot-Savart Law,

$$d\vec{B} = \frac{\mu_o}{4\pi} \frac{\vec{I\,ds} \times \hat{r}}{r^2} \text{,} \tag{2}$$

where $\vec{Ids}$ is a small current element and $\vec{r}$ is the distance from the current element to the field point. In this case, the configuration of the boundary current is such that the additional magnetic field contribution acts to increase the field inside the magnetopause and to cancel the magnetospheric field outside the boundary.

Treating the many incoming particles individually is an impractical method of arriving at an overall surface current configuration. Instead, these equations are combined with concepts in classical thermodynamics to arrive at equations of magnetohydrodynamics. The particular principle applied to calculate the shape of the magnetopause is to balance the incoming solar wind flux with the net magnetic scattering effect of the magnetospheric field. The magnetic field perpendicular to the boundary is presumably negligible. Equating the external plasma pressure on the boundary of the magnetosphere to the magnetic pressure of the

internal magnetic field at this location, the magnetohydrodynamic differential equation for the magnetosphere boundary is

$$\left|\hat{n}_s \times \vec{B}\right| \pm \hat{n}_s \cdot \hat{v} = 0 \tag{3}$$

where $\vec{B}$ is the net magnetic field at the boundary, $\hat{v}$ is the unit vector in the direction of the incident solar wind, and $\hat{n}_s$ is the unit vector normal to the magnetopause surface, given in spherical polar coordinates by

$$\hat{n}_s = K_n \left(\hat{r} - \frac{1}{r}\frac{\partial r}{\partial \theta}\hat{\theta} - \frac{1}{r\sin\theta}\frac{\partial r}{\partial \phi}\hat{\phi}\right) \tag{4}$$

with

$$K_n = \frac{1}{\sqrt{1 + \left(\frac{1}{r}\frac{\partial r}{\partial \theta}\right)^2 + \left(\frac{1}{r\sin\theta}\frac{\partial r}{\partial \phi}\right)^2}} \tag{5}$$

An initial magnetopause surface configuration is calculated using equation (3) with the magnetic field, $\vec{B}$, represented by interior field sources alone. After an initial three-dimensional zero-order surface has been constructed, the next step is to calculate the currents on that surface attributable to the deflected solar wind particles. These zero-order model surface current elements are computed using the following equation, where $\vec{B}$ is still the net interior sources' magnetic field:

$$\vec{J} = \hat{n}_s \times \vec{B} = \left(\frac{B_\theta}{r\sin\theta}\frac{\partial r}{\partial \phi} - \frac{B_\phi}{r}\frac{\partial r}{\partial \theta}\right)\hat{r} - \left(B_\phi + \frac{B_r}{r\sin\theta}\frac{\partial r}{\partial \phi}\right)\hat{\theta} + \left(B_\theta + \frac{B_r}{r}\frac{\partial r}{\partial \theta}\right)\hat{\phi} \tag{6}$$

The magnetic field arising from the computed current elements is then calculated by numerically integrating the Biot-Savart integral of the currents over the entire magnetopause surface, S', as follows:

$$\vec{B}_{n,SC} = \int \int dS' \, (\hat{n}_s \times \vec{B}_{n-1}) \times \frac{(\vec{r} - \vec{r}')}{\left|\vec{r} - \vec{r}'\right|^3} \tag{7}$$

Subsequent iterations again utilize Equation (3) to calculate the magnetopause, but now include the newly-calculated contributions of the surface currents in the net field, $\vec{B}$, at the boundary. This cycle continues, producing higher-order solutions, until no significant change in the magnetopause shape and surface current elements is observed for successive iterations. At this point, convergence is attained and the model is termed self-consistent.

In order to display the characteristics of the net magnetospheric model it is necessary to represent the magnetic field contributions of the magnetopause surface currents in a functionally continuous manner which is consistent with the Biot-Savart integrals over the surface current elements. These elements are generally computed on a 5° by 5° grid of the magnetopause surface. To achieve a functionally continuous representation for the entire space inside the magnetosphere, selections of calculated magnetic field components for a large number, N, of representative interior grid locations (r,θ,ϕ) are fit to the following Schmidt-normalized associated Legendre function expansion:

$$\Phi_S(r,\theta,\phi) = \sum_{n=1}^{n_{max}} r^n \sum_{m=0}^{n} G_{nm} P_n^m(\cos\theta) \cos(m\phi) \tag{8}$$

$$\vec{B}_S(r,\theta,\phi) = -\vec{\nabla}\,\Phi_S(r,\theta,\phi) \tag{9}$$

Φ_S is a scalar magnetic potential function of the surface current elements. The negative gradient of the potential function yields the magnetic field due to this source. Thus, given a set of interior field values and grid locations, coefficients G_{nm} are calculated such that the sum over the N values of the vector residuals squared is

minimized. This method follows the general technique set forth by *Mead and Beard* [1964] in their modeling of the Earth's magnetopause.

Self-consistent models for both the Pioneer-observed interior sources and the Voyager-observed interior sources have been published [*Engle and Beard*, 1980; *Engle*, 1991; *Engle*, 1992*a,b*]. In the latter Voyager models, a self-consistent magnetopause and surface current calculation was fit to an associated Legendre functions series of order n = 1 through n = 10. This expansion required sixty-five distinct coefficients, G_{nm}. For each of the magnetosphere models which lay the groundwork for our investigation, the development method was similar. However, until recently, the magnetopause surface calculation for each configuration assumed the magnetosphere surface current contribution to be that achieved by the idealized "no-tilt" calculation. The no-tilt assumption greatly expedited the achievement of self-consistency. Each of those calculations assumed the axis of all the interior sources of magnetic field to be perpendicular to the incident solar wind.

The rotation axis of Jupiter is tilted 3° with respect to the normal to the planet's orbital plane, and the magnetic axis makes an angle $\lambda = 10^{\circ}$ to the planet's rotation axis. As a result, the magnetic axis precesses about the planetary rotation axis during each diurnal rotation of period $9^{h} 55^{m} 41^{s}$. While ignoring the small tilt of the rotation axis, recent model calculations have incorporated the effects of the tilt of the magnetic axis relative to the incoming solar wind [*Engle*, 1992*b*]. A precession angle, α, is a useful parameter for describing the azimuthal orientation of the magnetic axis relative to

the incident solar wind. For the North magnetic pole tilted 10° toward the sun, $\alpha = 0^O$; tilted away from the sun (half of a rotation period later), $\alpha = 180^O$. Any given time during the Jovian day may be identified with a corresponding value of the precession angle, α.

Self-consistent models for each of eight values of α, at 45° intervals, have been constructed by means of the iterative method described above. Similar processes may be performed for any static model corresponding to any particular assigned precession angle orientation. The details of the models for $\alpha = 0^O$ and $\alpha = 180^O$ have already been published [*Engle*, 1992*b*].

IV. Developing a Time-dependent Model

The limiting feature of these models is their inherent static nature. Field characteristics at a given location can be derived with considerable accuracy, but the procedure demands an inordinate amount of time. For any given precession angle, the Schmidt-normalized spherical harmonic expansion must be refit to observations, and new coefficients of the harmonic expansion must be calculated. A more valuable model would be one which provides a complete model description of the magnetic field associated with the diurnally varying Jovian magnetopause, a model which is functionally continuous in time as well as in position. Such a model would provide a magnetic description of any point within the magnetosphere at any time during the Jovian day.

A simple dipole and a co-rotating current sheet produce field components which are relatively simple to model in a time-dependent manner. Both sources are modeled to be symmetric

about the magnetic axis. In accounting for the tilt of this axis, the field components need simply to be translated from a sinusoidally-varying reference frame into a fixed frame defined by a rotation axis which is approximately normal to the orbital plane of the planet. The crux of a complete time-dependent model lies in the complexity of coupling the iterative calculation of the surface current field source to the precession of the magnetic axis about the rotation axis.

Associated Legendre functions were appropriately used to describe the magnetic potential due to currents on the magnetopause. The coefficients, G_{nm}, act to weight each of the associated Legendre functions which, collectively, map this magnetic potential. As the magnetic axis precesses, these functions must be combined in different proportions to reflect the dynamics of the magnetopause and the resulting surface currents. These coefficients introduce the variation which allows this field to change with the precession of the magnetic axis, α.

Since each complete rotation must bring the field back to its original state (assuming the constancy of parameters such as solar wind strength and sheet current density), these coefficients assume a functional form which is dependent on the precession angle and is necessarily periodic in nature. In the absence of well-developed evidence to the contrary, the coefficients are also assumed to be symmetric for precession angles which are symmetric with respect to the noon-midnight meridian plane.

This assumed symmetry was a fundamental assumption of the Pioneer and Voyager magnetometer teams and underlies the work of these teams. There is some speculation that the sheet current

undergoes expansion and compression as it moves from the more closely-confined day-side to the more expansive night-side of the magnetosphere and back again. Other related considerations are that the precession of the current sheet may lag that of the planetary dipole by some fixed azimuthal angle or that the current sheet may undergo differential rotation about the planet (rotating at smaller angular velocities at greater distances from the planet). These ideas, if correct, may introduce some deviation from the assumed symmetry of the magnetopause and the surface current contribution. Analysis of Ulysses magnetometer data may provide further insight into these phenomena in the near future.

Included in the complete Voyager Jovian magnetosphere model published at static precession angles of 0° and 180° [*Engle* 1992*b*] are the corresponding Legendre function expansion coefficients for both orientations. Using the magnetospheric surfaces and associated grid of surface current elements for each of the values of the precession angle $\alpha = 0^{\circ}$, 45°, 90°, 135°, 180°, 225°, 270°, and 315°, expansion coefficients were computed for eight orientations of the magnetic axis equally spaced over the course of a Jovian day. In each case, Legendre functions of order one through ten were used to maintain the self-consistency of the surface current structure. The result was eight sets of sixty-five values, each value acting to weight a particular associated Legendre function in constructing the magnetic field components for a given precession angle. This data was regrouped into sixty-five sets of eight values, so that each set now represented the variation of one particular coefficient over the course of a day. Appendix A displays these coefficients.

Each of these sets was then graphed as $G(n,m,\alpha)$ versus α and was studied for an inherent pattern. A concise mathematical representation of each coefficient would enable smooth interpolation between any two of the eight adjacent (in α), self-consistent magnetic field representations. Most of these self-consistent model coefficients were, in fact, approximately symmetrical with respect to the noon-midnight plane. One such example is displayed in Figure 4.

Figure 4. Variation of the associated Legendre function expansion coefficient $G(4,0,\alpha)$ as a function of the precession angle of the magnetic axis.

Coefficient produced by the self-consistent model

Functional approximation of the coefficient

Precession angle, α (in radians)
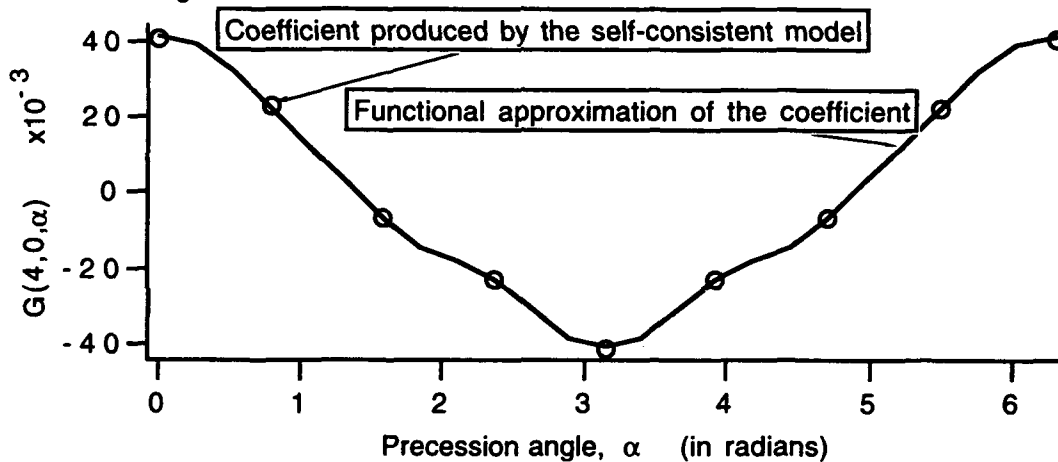
In some cases, the patterns were more difficult to represent functionally, as indicated by Figure 5.

Figure 5. Variation of the associated Legendre function expansion coefficient $G(5,5,\alpha)$ as a function of the precession angle of the magnetic axis.

Coefficient produced by the self-consistent model

Functional approximation of the coefficient

Precession angle, α (in radians)
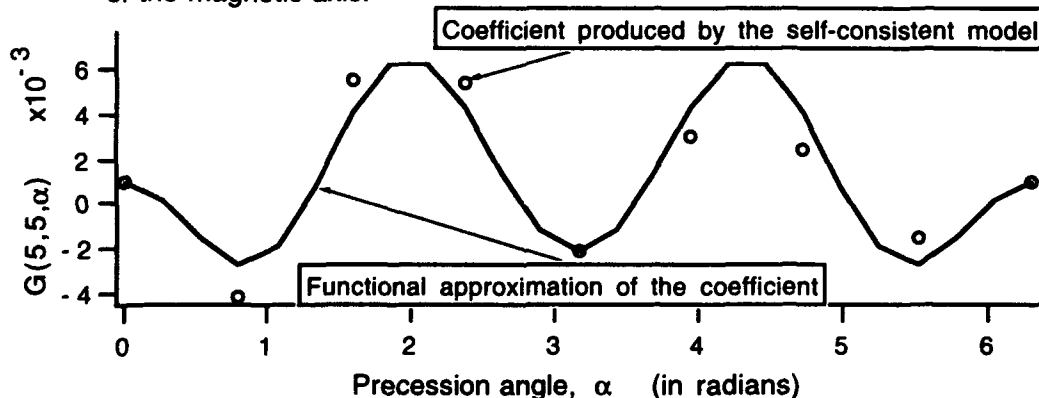
The fitting of the surface current representation to the expansion coefficients G_{nm} for each static model was somewhat sensitive to the particular selection of computed field components. For this reason, we considered each data point, $G(n,m,\alpha)$, to have some range of uncertainty. For each graph, a unique periodic function was developed which would, ideally, intercept the eight self-consistent model points. However, none of the sixty-five coefficients was precisely symmetric over the course of a day. Often, two precession angle orientations which were symmetric with respect to the noon-midnight meridian plane yielded slightly different values for a given coefficient. In such a case, the corresponding functional representation assumed an average value of the coefficient for both orientations. For precession angles between any two of the eight self-consistent model values, each function traced a path which would reasonably approximate the variation of the coefficient over the corresponding range of precession angles.

Initially, different functional forms were used to model different coefficients, $G(n,m,\alpha)$. However, this experimentation proved a fifth-order cosine series, a symmetric and periodic function, to be capable and practical for describing most of the sixty-five expansion coefficients. Actually, the precise form of the function was inconsequential. The aim was to achieve a reasonable mathematical description of each coefficient, and clearly there was no unique solution. The final functional forms of each coefficient are listed in Appendix B. Using these time-dependent coefficients, the Voyager-based model was streamlined and the laborious procedure detailed above for calculating the magnetopause structure for a given

precession angle was made obsolete. Fortran-based computer programs had previously been developed by Engle to construct the magnetopause and perform the least-squares fitting to the associated Legendre functions. With the functions $G(n,m,\alpha)$ substituted into the original program structure, the model could now calculate the Voyager Jovian magnetospheric field at any point within the magnetosphere (r,θ,ϕ) and at any precession angle, α. This representation adds a functional estimate of the magnetopause surface current contribution to the two interior sources of the planet's field.

V. Testing the Model

The new model's utility in describing the Jovian magnetosphere environment had yet to be demonstrated. Clearly, the functions developed to model the coefficients did not precisely match the self-consistent coefficients point for point. The pertinent assumption was that any deviations would be small and, averaged over the sixty-five functions, inconsequential. Thus, the new model should produce time-dependent values which approximately incorporate and maintain the self-consistency of the old models.

Utilizing the new time-dependent model software, a second Fortran-based program generated the coordinates of individual magnetic field lines emanating from the surface of Jupiter. To investigate the physical nature of these field lines, hundreds of similar lines were graphed, originating at a wide spread of locations on the surface of Jupiter for numerous values of the precession angle.

Figure 6 shows the field lines ori inating in the noon-midnight
meridian plane ($\phi = 0^\circ$) for a preces: angle, $\alpha = 60^\circ$.

Figure 6. Noon-midnight plane projection of selected magnetic field lines
of the Jovian magnetosphere at a precession angle, $\alpha = 60^\circ$
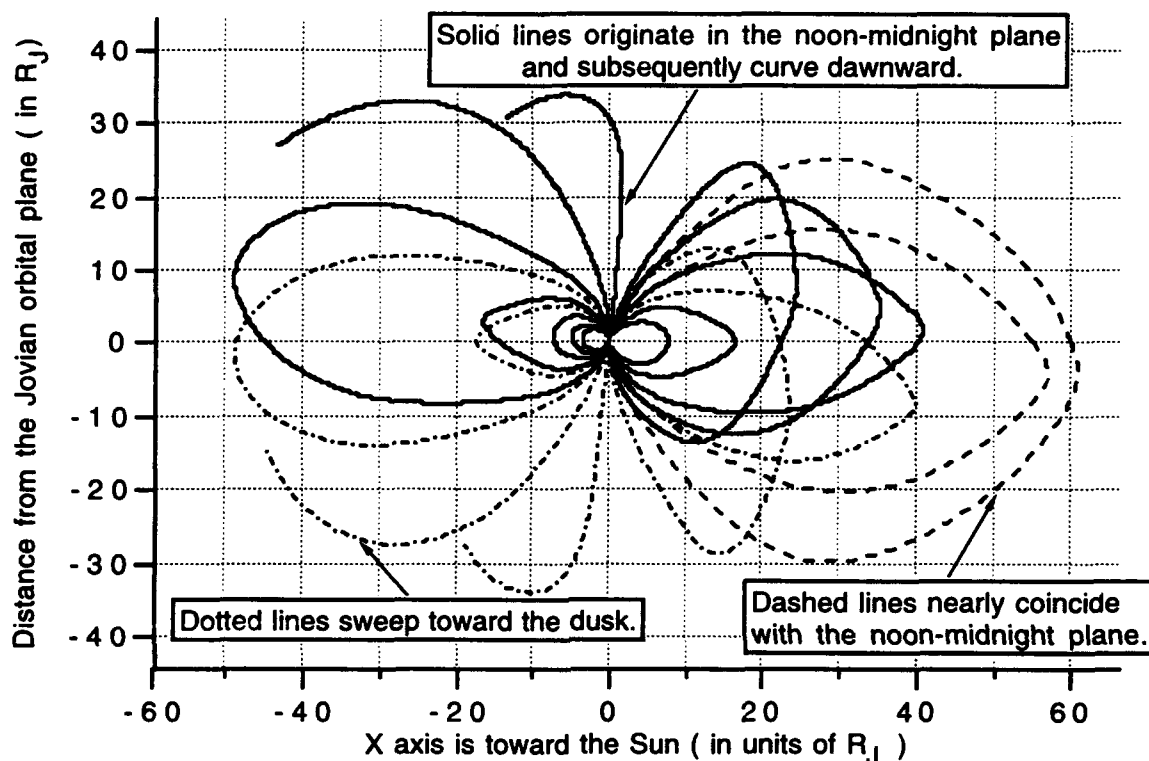
The goal was to ensure that families of magnetic field lines predicted
by the time-dependent model were, in fact, physically realistic. A
well-behaved line would be smooth and continuous and would not
cross any of its neighboring field lines. Of particular interest were
those lines originating near the cusp regions. The two cusp regions
(clearly displayed in Figure 3) are the "effective" magnetic poles of
the magnetospheric field. Magnetic field lines branch out from the
northern cusp and return to the southern cusp. The true magnetic
poles are at opposite extremes of the planet, but the interaction of
the solar wind causes these cusp regions to be swept sunward from

the poles. Magnetic field lines emanating from these points closely parallel the magnetopause and, if modeled incorrectly, will tend to deflect outside of the magnetopause, representing nonphysical field components outside of the magnetosphere region.

In calculating magnetic field lines, those which extend beyond 70 R_J from the planet are discontinued at $r = 70$ R_J to reflect only the range over which reasonably reliable field predictions are expected. Voyager 2 observations indicated a subsolar point of about 60 R_J. In the tilted models, the subsolar point is the radial position, measured in the magnetic equatorial plane, which is closest to the Sun. This point is the reference position for the spherical harmonic expansion of the Voyager-based model. The magnetic potential within the day-side magnetosphere region lends itself well to this functional description, and the night side is modeled reasonably well within about 60 - 70 R_J. However, as the night-side magnetosphere widens and extends millions of miles in the anti-solar direction (and hence, outside of a spherical boundary of $r = 60$ R_J), the associated Legendre function representation is decreasingly reliable in the modeling of the magnetic potential.

VI.   The Trajectory Test

Obvious programming errors were eliminated under the scrutiny of the telltale magnetic field line traces. The qualitative result was a physically realistic time-dependent description of Jupiter's magnetospheric field. A more stringent test, of course, would address the quantitative nature of the model. How well does it predict magnetic field values in the vicinity of Jupiter?

Unfortunately, means for comparison were limited. Until the recent Ulysses mission, only four spacecraft had traced trajectories through the Jovian magnetosphere, each equipped with magnetometers which measured the magnetic field in spacecraft-centered rectangular coordinates. Each of these explorers was limited to a pass near the orbital plane of the planet, leaving the higher latitudes unexplored. Nonetheless, Voyager 2 data provided a reasonable control against which to check the accuracy of the time-dependent model. This data, in particular, was chosen because the model assumed the parameters for solar wind strength, subsolar point, and sheet current density which were consistent with Voyager 2 observations.

On board Voyager 2, field component measurements were taken every sixty milliseconds. For practical purposes, these measurements were averaged over forty-eight second intervals, 1800 data points per Earth calendar day. Position determinations were made separately and followed roughly one second after the corresponding averaged field readings. This data was translated into Jupiter-centered rectangular coordinates, with the x-axis in the direction of the Sun and the z-axis perpendicular to the planet's orbital plane. Coupling the lagging position measurement to the leading field measurement, these readings were treated as though they had been taken simultaneously. This approximation did not introduce any significant error.

Magnetometer readings on 5 and 6 July, 1979, revealed that the spacecraft was experiencing Jupiter's bow shock, evidenced by magnetic "noise" on the order of 5 - 10 nT. The bow shock is a supersonic shock wave, a dynamic buffer region which envelops the

deflected solar wind particles and separates the interspace medium from Jupiter's magnetosphere. The bow shock is characterized by turbulent flow of the deflected solar wind particles. The spacecraft crossed the magnetopause early on the 6 July. Unfortunately, data from the Voyager on 7 July never reached Earthbound receivers. This limits our control data to a range between 8 July, when Voyager 2 was inbound at about 33 R_J from Jupiter, and 14 July, when the Voyager was outbound on the anti-solar side at about 72 R_J from Jupiter. Figure 7 shows the trajectory of Voyager 2 as the position data was received by earthbound receivers.

Figure 7. 1979 Jupiter-encounter trajectory of Voyager 2 in planetocentric orbital coordinates. The x-y plane lies in the orbital plane of the planet.
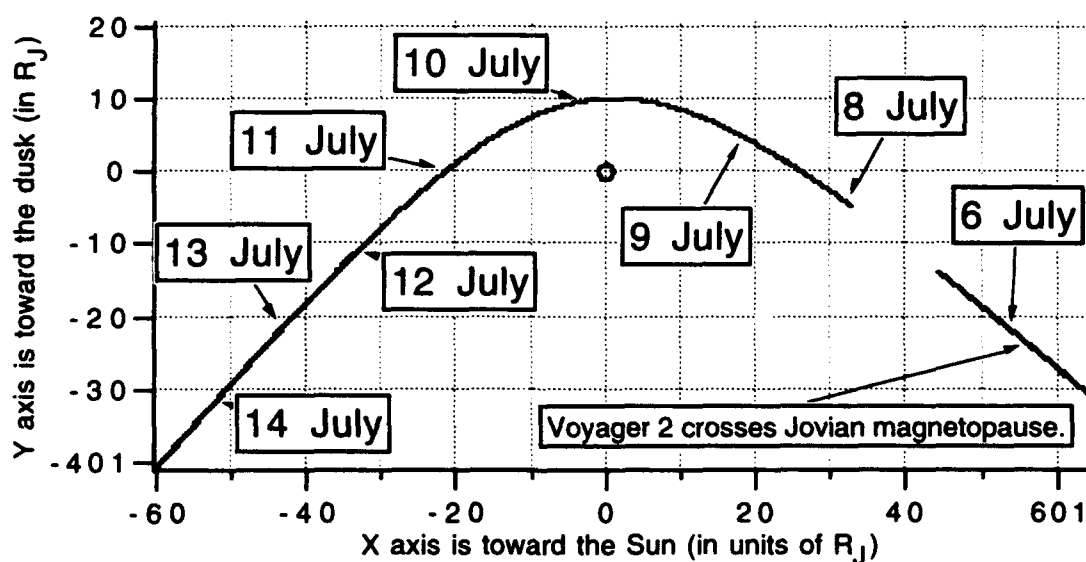
A few other clearly erroneous position and field measurements were excluded from this display and from the following data analysis. In addition, reports of initial Voyager 2 observations [Ness et al., 1979] indicate that some data from 8 July may be tainted by an apparent tumbling of the spacecraft which was unaccounted for in subsequent

reference frame translations. The magnitude of the net field observed on this day is, of course, still reliable, but components of the field may not be accurately decomposed.

The reported position data were translated into Jupiter-centered spherical coordinates and the resulting data set was used as position input to the time-dependent magnetosphere model. Again, Fortran-based programs were used to handle the enormous volume of data. The model calculated the magnetic field components (B_r, B_θ, B_ϕ) in spherical coordinates for each data point along the Voyager trajectory. Incorporated in the model is the rotational rate of Jupiter, $360^\circ/(9^h\ 55^m\ 41^s)$, which equates to 0.483480° every forty-eight seconds (each position interval).

It was necessary to assume an initial precession angle, a reference orientation for the first trajectory position on 8 July. At each subsequent trajectory point, the model would update the precession angle based on the planetary rotation rate and would then calculate the magnetic field components. An initial precession angle $\alpha_i = 210^\circ$ at 00^h00^m 8 July was chosen such that the magnetic axis was tilted directly toward the sun at 00^h00^m of the day of Jupiter's closest approach to the planet, 9 July. This arbitrary choice was a matter of convenience. The ensuing field calculations provided grounds for calibrating this assumed initial precession angle with spacecraft observations.

Next, the Voyager-observed field measurements were translated into a form which was comparable with model calculations. A Fortran-based program utilized the same spacecraft position data file which was employed by the time-dependent model,

but it also converted the corresponding observed field component measurements (B_r, B_θ, B_ϕ) into a Jupiter-centered spherical coordinate system with $\phi = 0^O$ toward the Sun.

Because the Voyager 2 trajectory paralleled Jupiter's orbital plane, the spacecraft encountered the planet at locations in and near the magnetic equatorial plane. The precession of the magnetic axis caused the co-rotating current sheet to repeatedly cross the spacecraft trajectory. Hence, the Voyager's Jupiter-centered coordinates alternated between the northern magnetic hemisphere and the southern magnetic hemisphere during the course of each day. Referring to the field line plot in Figure 3, it is clear that magnetometer readings of the component B_r should indicate alternating positive and negative values as the Voyager 2 entered the northern and southern magnetic hemispheres, respectively. When the magnetic axis was tilted away from Voyager 2, $|\alpha-\phi| > 90^O$, field lines were directed radially inward to the planet, while a tilt toward the Voyager, $|\alpha-\phi| < 90^{O,}$ caused f eld lines to point radially outward.

The nearly periodic nature of the B_r component provided a simple means to calibrate an initial precession angle. The assumption that $\alpha_i = 210^O$ had resulted in B_r component calculations which were almost exactly 180° out-of-phase with spacecraft observations. Rotating the magnetic axis forward 180.2^O in its precession put model calculations of the current sheet crossings in phase with spacecraft observations. Setting $\alpha_i = 30.2^O$ at 00^h 00^m on 8 July, the model was again used to predict the field components along the following seven days' journey through the magnetosphere.

The model values and observed values of the B_r component on 9 July are overlaid in Figure 8.

Figure 8. Model and observed magnetic field components directed radially outward from Jupiter on 9 July, 1979.
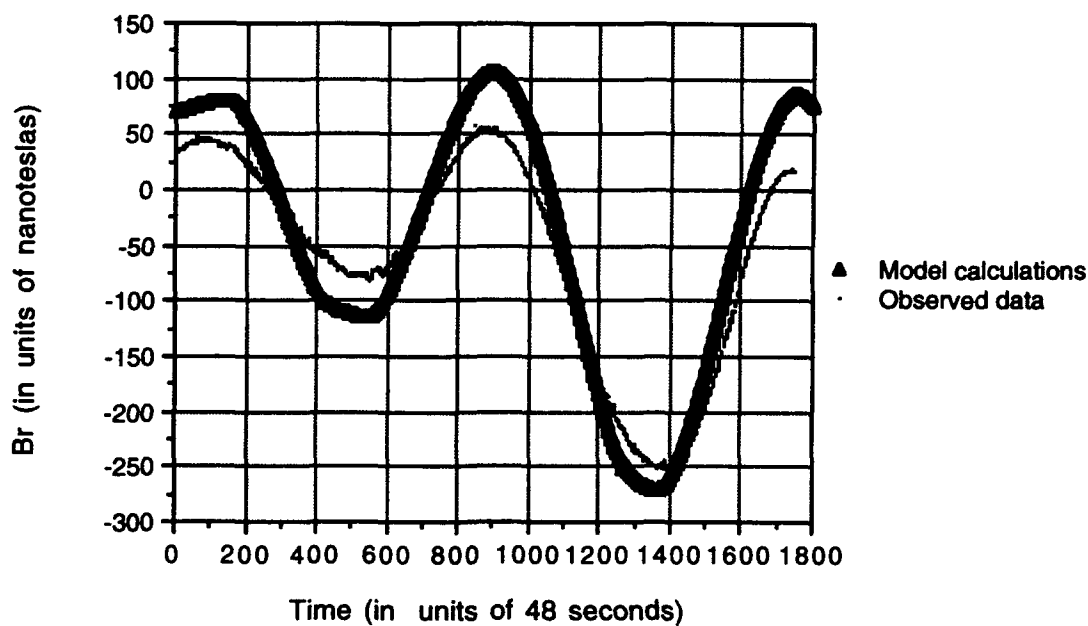
The agreement between theory and experiment is remarkable. The model accurately portrays the sheet current crossings and also predicts values for B_θ which nearly coincide with the observed values. While the variation in B_r closely matches observation, the model does predict a greater range of magnitudes than are observed for this field component. Curiously, B_ϕ seemed to be 180° out of phase with observations, although the much smaller magnitude of the B_ϕ component made comparisons more difficult and less meaningful.

VII.   Calibration and Some Deductions

Voyager 2 observations were useful in substantiating what was now the first mathematical description of the Jovian magnetosphere to incorporate the continuous diurnal variation of the magnetopause current contributions.   Model calculations proved to be reasonably consistent with spacecraft observations.   Through a closer comparison of these data sets, an assessment of various model parameters can be made, leading to improvements in the model and deductions about the actual magnetic field source structure.   Several attempts were made to optimize the fit of the model to Voyager observations through the variation of model parameters.   Some conclusions derived from these efforts follow.

Figure 9 displays the model values and the observed values of the B_r component over the entire trajectory data set, 8 - 14 July.

Figure 9. (a) Model magnetic field components directed radially outward from Jupiter from 8-14 July, 1979.
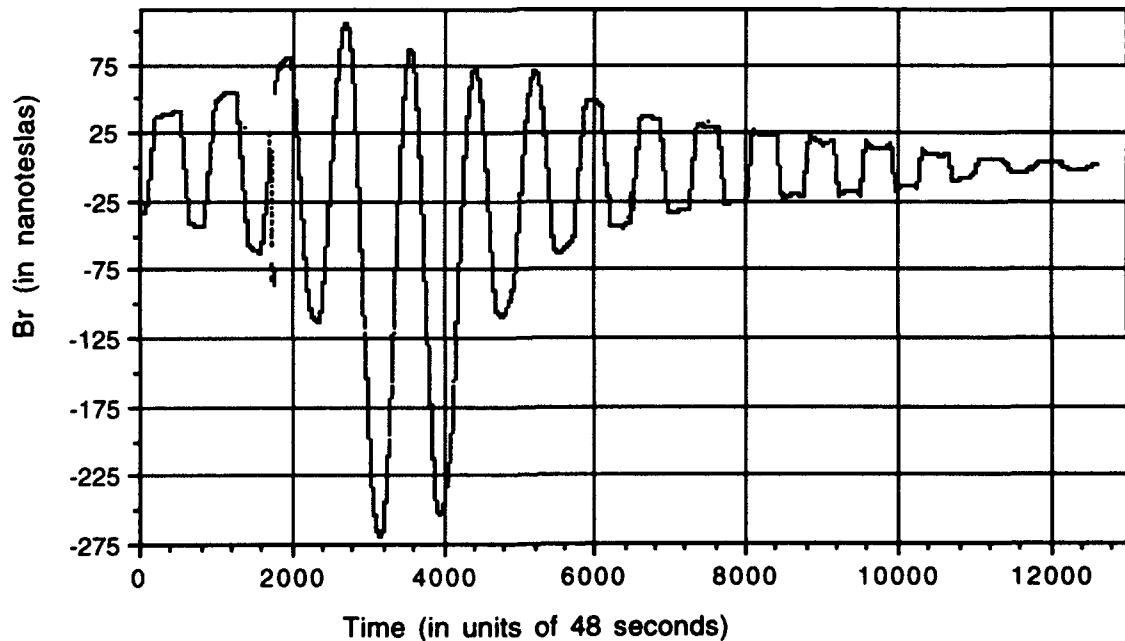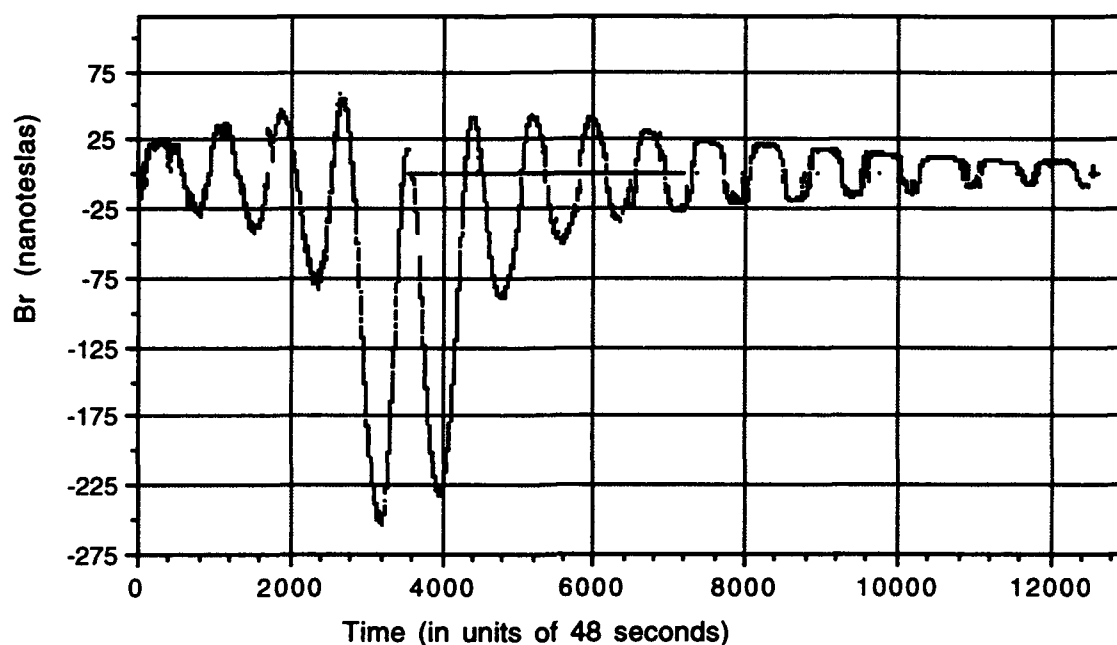
Figure 9 (b) Voyager-observed magnetic field components directed radially outward from Jupiter from 8-14 July.

The precise agreement of the model's predicted current sheet crossings with the Voyager-observed crossings (where $B_r = 0$, we infer that Voyager 2 crossed the center of the current sheet) substantiates the concept of a rigid current sheet. This is significant because there has been some speculation in recent years that this current sheet is not rigid but actually experiences differential rotation about the magnetic axis. This would entail the current sheet rotating with slower angular velocity as distance from the planet increases. If this were the case, Voyager 2 would not have recorded the consistent periodicity of the sheet crossings which is indicated by the both the spacecraft data and the rigid current sheet model (incorporated in the time-dependent model). The fact that it did measure this periodicity is confirmation of the rigidity of the sheet current structure.

On 12 July, the Voyager 2 made the subtle transition into the magnetotail region of Jupiter, where it remained for the following two days of our data set. Stretching millions of kilometers in the anti-solar direction, the magnetotail region is defined by electromagnetic phenomena which are not properly addressed by the magnetosphere model. Within a radial distance of about 35 R_J in the anti-solar direction, current sheet crossings occurred nearly coincident with the spacecraft traversal of the magnetic equatorial plane. As the outbound spacecraft approached the pre-dawn magnetosphere, however, south-to-north sheet crossings occurred with less regularity. This phenomenon has been previously noted and is generally understood in terms of a "periodic rocking of the tail current sheet about the longitudinal axis of the tail, as Jupiter rotates". [*Ness et al.*, 1979] The magnetotail region is, in fact, a distinctly different region of magnetic activity which is not addressed by models of the Jovian magnetosphere. In this region, larger discrepancies were noted between model calculations and Voyager 2 observations than during previous days when the spacecraft was nearer the planet.

In an attempt to optimize the fit of the model to Voyager observations, maximum likelihood theory was applied to the variation of several model parameters. Variation of the initial precession angle led to further deductions about the Jovian magnetic field source structure. Based on the visually calibrated initial precession angle, $\alpha_i = 30.2^O$, χ^2 calculations of B_r, B_θ, B_ϕ and B_{total} were performed using methods consistent with those outlined by

Taylor [1992]. χ^2 values for each field component $(\chi^2_r, \chi^2_\theta, \chi^2_\phi)$ were calculated for each of several assumed initial precession angles.

Taken individually, these calculations meant very little. However, a comparison of the χ^2 values from each of several closely-spaced initial precession angles provided a relative comparison of the model's ability to match the observed results for a given α_i. This could make possible a more accurate calibration of the initial precession angle by seeking a minimum value of χ^2 over the 360° range of values for the initial precession angle. The results were surprising. χ^2_r was minimized for $\alpha_i = 67.2 \pm 0.5°$. This angle is displaced 37° from the visually calibrated initial precession angle, $\alpha_i = 30.2°$. A careful inspection of the software revealed no programming errors, but neither can this discrepancy be positively attributed to any other cause.

The minimum χ^2_θ value occurred for an angle, $\alpha_i = 28.2 \pm 0.5°$, 39° displaced from that for the minimum χ^2_r calculation. Near Jupiter's orbital plane, the B_θ component is strongly influenced by the orientation of the magnetic axis. The B_r component, on the other hand, is overwhelmingly the product of the co-rotating current sheet. Disparate minimum χ^2 calculations could indicate that the two internal field sources--the planetary dipole and the co-rotating current sheet--are out of phase. In other words, the current sheet might lag the magnetic axis in its precession.

Inferences drawn from the χ^2 calculations are by no means conclusive. Reservations about these deductions stem from the observation that the minimum χ^2_r value does not correspond to the

visually calibrated initial precession angle. Nonetheless, the ideas which are presented demand consideration as genuine physical phenomena of the Jovian magnetosphere system. The time-dependent nature of this model makes it particularly useful in the analysis of these and similar experimental observations.

VIII.   Future Tests

While a new magnetosphere model may fit observed data somewhat better, this is no guarantee that the model itself is better. The essential question of a model's utility is how well it predicts field properties at points not on the Pioneer and Voyager trajectories, nearer Jupiter or at higher or lower latitudes, for example.

Average sheet current density, subsolar point and other model parameters were reported for the Pioneer 10 and 11 flybys as well as both Voyager flybys. Substituting Pioneer-deduced parameters for those of the Voyager mission which currently define the time-dependent model, we should achieve a reasonable approximation of the magnetic environment encountered in 1973 and 1974 by Pioneer 10 and 11.

More recently, in 1992, the spacecraft Ulysses encountered Jupiter en route to its sweep of the polar regions of the Sun. The data collected at Jupiter, which has not yet been released for public use, will provide another control against which to gauge the value of the Voyager-based time-dependent model. Because Jupiter was used in a gravity boost maneuver to deflect Ulysses out of the solar ecliptic plane and into a polar orbit of the Sun, measurements from Ulysses spanned a much wider range of Jovian latitudes and provided a more

complete sampling of the planetary magnetic field than any previous mission to the planet. Data from this mission can be gainfully compared to the predictions of our time-dependent model along the spacecraft trajectory.

IX.   Application of the Model

Perhaps the most interesting application of the new time-dependent model involves the upcoming July 20, 1994 collision of comet Shoemaker-Levy 9 with Jupiter. A team headed by Principal Investigator Renee Prange, of the Institut d'Astrophysique Spatiale at the University of Paris, ORSAY, France, has been awarded telescope time on the Hubble Space Telescope during the time of the comet's pass through the Jovian magnetosphere. This team will image the enhanced particle activity which results when ions from the comet's corona encounter the magnetic field of Jupiter.

As the comet crosses the Jovian magnetopause, the charged particles which constitute the comet's corona will be subject to the same magnetic force which describes the solar wind deflection at the magnetopause boundary. These particles will undergo a cyclotron process, spiraling up and down the magnetic field lines which cross the comet ephemeris, or trajectory.

At the request of Prange, and based on the predicted comet trajectory positions which she provided, Engle originally used the static self-consistent model to calculate the magnetic field lines anticipated to lie along the comet ephemeris. More recently, the time-dependent model has been applied to the trajectory for a wide range of magnetic axis precession angles to locate and map these

predicted magnetic field lines. The results have been sent to the observation team.

Figure 10 displays two characteristic magnetic field line calculations corresponding to the 17.5 July (12^h 00^m on 17 July) and 18.2 July (04^h 48^m on 18 July) positions of Shoemaker-Levy 9.

Figure 10. Comet Shoemaker-Levy 9 ephemeris with selected calculated magnetic field lines for $\alpha = \phi$.
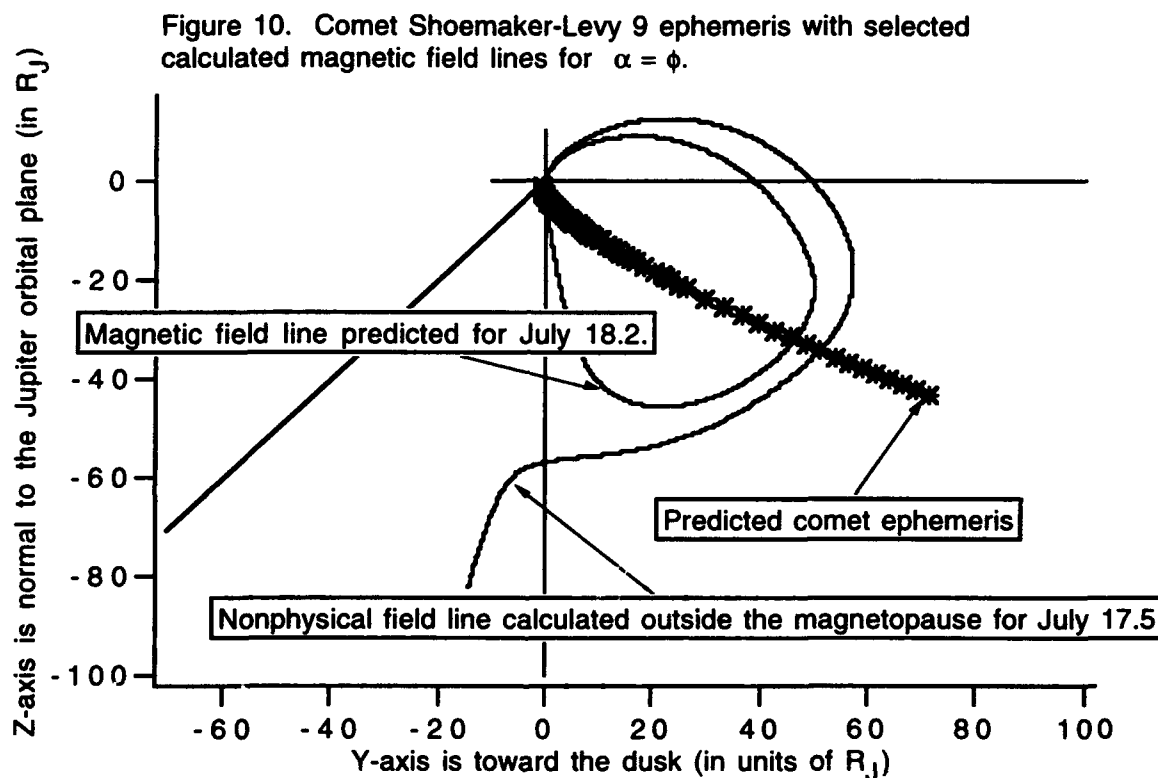
The first line encountered on the inbound trajectory fails to close on the planet, indicating that the comet is close to crossing the magnetopause. The magnetosphere model is only valid for points within the magnetopause. For points just outside the boundary, the model breaks down and predicts field lines which fail to close. The second line does eventually close on the planet, indicating that, at this location and precession angle, the comet will have entered the magnetopause. These and similar field predictions should help the

team to anticipate the times and regions of enhanced particle activity within the magnetosphere.

The expected particle activity is of particular interest to physicists studying the comet's composition. Current theory places the origin of comets in a spherical shell, or cloud, some 50,000 AU, or 7.48 (10^{12}) km, from the Sun [*Chaisson and McMillan*, 1993]. Because this cloud is believed to be left over from material that condensed to form the solar system, the composition of comets should reflect the composition of the original solar nebula. Imaging the evaporated, ionized constituents of the comet Shoemaker-Levy 9 should yield significant information about this composition.

X. Conclusions

Among the benefits of the time-dependent representation is its ability to produce a "living" model of the complete magnetosphere of Jupiter, including those regions which are near to the magnetopause and those which vary substantially in their field properties with the precession of the magnetic axis. The model stands up to the qualitative requirement that it produce physically realistic magnetic field lines. It also yields field component calculations which are quantitatively consistent with Voyager 2 magnetometer readings.

Clearly, the time-dependent magnetosphere model is already providing a service to the space-science community. The model has been used to provide insight into the upcoming interaction of comet Shoemaker-Levy 9 with the Jovian magnetosphere. In upcoming months, this model may also serve an important role in the analysis of the recent Ulysses spacecraft encounter data and of the upcoming

Galileo observations. In these and other future encounters with Jupiter, a time-dependent model can render far less formidable the task of reconciling large volumes of data in the form of magnetic field component measurements to models which include all the basic salient features of the magnetospheric environment. This allows a more reliable separation of phenomena between those which are inherently characteristic of a dynamically stable, albeit diurnally varying, magnetosphere and those which are transient perturbations in the magnetospheric field.

Developed as an extension of existing Voyager-based representations, the time-dependent model reflects the effects of nearly maximum solar wind pressure conditions. However, the model should provide a guide to analogous representations for the magnetopause surface current contributions resulting from minimum solar wind pressure conditions (as observed by the Pioneer spacecraft) and solar wind pressure conditions between the two extremes.

A time-dependent representation should be valuable to experimenters who directly measure characteristics of the plasma particles encountered during spacecraft flybys. These particles are charged and are, thus, sensitive to the magnetic field environment through which they move. Knowledge of the magnetic field environment experienced by those particles just prior to their observation is essential to being able to draw inferences regarding the overall population of the plasma environment from the small sample actually observed.

Acknowledgements

I am extremely grateful to:

REFERENCES

Chaisson, Eric, and Steve McMillan, *Astronomy Today*, Prentice Hall, p. 336, 1993.

Connerney, J. E. P., M. H. Acuna, and N. F. Ness, Modeling the Jovian Current Sheet and Inner Magnetosphere, *J. Geophs. Res.* **86**: 8370, 1981.

Connerney, J. E. P., M. H. Acuna, and N. F.Ness, Voyager 1 Assessment of Jupiter's Planetary Magnetic Field, *J. Geophs. Res.* **87**: 3623, 1982.

Engle, Irene M., and David B. Beard. Idealized Jovian Magnetosphere Shape and Field, *J. Geophys. Res.* 8ⁿ, 579-592, 1980.

Engle, Irene M., Idealized Voyager Jovian Magnetosphere Shape and Field, *J. Geophys. Res.* **96**, 7793-7802, 1991.

Engle, Irene M., The Field of the Jovian Magnetosphere, Including Contributions of the Magnetospheric Surface Currents, *Adv. Space Res.* Vol. **12**, No. 8, pp. (8)249-(8)255, 1992 (a).

Engle, Irene M., Diurnal Variations in Jovian Subsolar Position, *J. Geophys. Res.*, **97**, pp. 17169-17172, 1992 (b).

Ness, N. F., M. H. Acuna, R. P. Lepping, L. F. Burlaga, K. W. Behannon, and F. M. Neubauer, Magnetic Field Studies at Jupiter by Voyager 2: Preliminary Results *Science* **206**, 966, 1979.

Smith, E. J., L. Davis, Jr., D. E. Jones, P. J. Coleman, D. S. Colburn, P. Dyal, C. P. Sonett and A. M. A. Frandsen, The planetary magnetic field and magnetosphere of Jupiter: Pioneer 10, *J. Geophs. Res.* **79**, 3501, 1974.

Taylor, John R., *An Introduction to Error Analysis*, Oxford University Press, p. 162, 1982.

Appendix A

Associated Legendre Function Expansion Coefficients G(n,m) for Each of Eight Distinct Values of the Precession Angle, α

	$\alpha=0^\circ$	$\alpha=45^\circ$	$\alpha=90^\circ$	$\alpha=135^\circ$
G(1, 0)	-0.58087701	-0.58464450	-0.59458369	-0.61738110
G(1, 1)	-0.08373246	-0.10518049	0.01739297	0.09397754
G(2, 0)	0.01284187	-0.00414274	-0.00586055	0.01140946
G(2, 1)	-0.34831586	-0.31549028	-0.31097990	-0.34939179
G(2, 2)	-0.04608620	-0.02888788	0.00147852	0.04055239
G(3, 0)	-0.07753199	-0.09483284	-0.06431898	-0.08158017
G(3, 1)	-0.04682504	-0.04671578	-0.00771004	0.05568385
G(3, 2)	-0.07688551	-0.05731300	-0.05547160	-0.07043299
G(3, 3)	-0.01007293	-0.00457890	-0.00789330	0.01073236
G(4, 0)	0.04050628	0.02233014	-0.00737017	-0.02311350
G(4, 1)	-0.14027660	-0.14176409	-0.11574018	-0.13151264
G(4, 2)	-0.02936912	-0.04489575	0.00505519	0.04719570
G(4, 3)	-0.00192175	-0.00283145	0.00963413	-0.00178103
G(4, 4)	-0.00026736	-0.00609120	0.00217616	0.00336623
G(5, 0)	-0.00440191	-0.00285284	-0.00698109	-0.00666580
G(5, 1)	-0.01023021	-0.02333847	-0.00371074	0.01137838
G(5, 2)	-0.06185311	-0.07630672	-0.07628365	-0.05615139
G(5, 3)	0.00137553	-0.01738635	-0.00019316	0.03860091
G(5, 4)	-0.00061794	-0.01071075	-0.00189747	-0.00169872
G(5, 5)	0.00102967	-0.00419982	0.00550852	0.00543485
G(6, 0)	0.02902861	0.02742495	0.00004615	-0.01623161
G(6, 1)	-0.06302944	-0.04277107	-0.04756158	-0.04363710
G(6, 2)	-0.02455459	-0.02079814	-0.00113889	0.02152534
G(6, 3)	-0.00076756	-0.02664453	-0.03697173	-0.02952027
G(6, 4)	-0.00107624	-0.00697785	-0.00109286	0.01247352
G(6, 5)	-0.00561647	-0.00695962	-0.01348485	-0.01886771
G(6, 6)	0.00107300	-0.00135418	0.00238792	0.00654377
G(7, 0)	0.02305909	-0.00585131	0.01376711	-0.00308078
G(7, 1)	0.01690746	0.00244996	-0.00784696	-0.01351918
G(7, 2)	-0.04826577	-0.02443572	-0.03400584	-0.02146269
G(7, 3)	-0.00287149	-0.01368837	-0.00230085	0.03535789

	$\alpha=0^o$	$\alpha=45^o$	$\alpha=90^o$	$\alpha=135^o$
G(7, 4)	0.00951634	-0.00662937	-0.01500556	0.00283014
G(7, 5)	-0.00450697	0.00265004	-0.00212342	0.01161497
G(7, 6)	-0.00153519	-0.00394044	-0.00729356	-0.02680986
G(7, 7)	-0.00008509	-0.00136553	-0.00534947	0.00755032
G(8, 0)	-0.00228506	0.00402767	0.00619260	0.00134180
G(8, 1)	0.00010531	-0.00015627	0.00008461	-0.00014980
G(8, 2)	-0.00001137	-0.00005795	-0.00005257	-0.00013253
G(8, 3)	-0.01632791	-0.01880890	-0.01655571	-0.02296084
G(8, 4)	0.00142376	-0.00287784	-0.00165362	0.00526673
G(8, 5)	0.00022744	-0.00167888	-0.00569675	-0.00353761
G(8, 6)	-0.00185125	0.00163802	0.00386679	-0.00120294
G(8, 7)	-0.00000794	-0.00224809	0.00012707	-0.02030550
G(8, 8)	-0.00048340	-0.00257745	-0.00344984	-0.00020140
G(9, 0)	0.01475084	-0.05063475	0.01543967	-0.02427792
G(9, 1)	-0.00004873	0.00028903	0.00020044	-0.00141558
G(9, 2)	-0.00024329	0.00028468	-0.00106705	0.00093716
G(9, 3)	-0.00069491	-0.00629399	0.00633331	0.01209011
G(9, 4)	-0.00112535	-0.00821168	-0.01420589	0.00618697
G(9, 5)	0.00022736	-0.00199628	-0.00367437	0.00925356
G(9, 6)	-0.00053356	-0.00252830	-0.00212323	-0.00332920
G(9, 7)	-0.00024186	0.00325698	0.00384551	-0.00118829
G(9, 8)	-0.00002757	0.00038692	0.00068225	-0.00764674
G(9, 9)	-0.00032792	-0.00061381	-0.00022198	-0.00432999
G(10, 0)	0.00001903	0.00002531	0.00001285	0.00070200
G(10, 1)	0.00013265	-0.00101637	0.00048879	-0.00040118
G(10, 2)	-0.00011846	-0.00003653	-0.00062103	0.00015092
G(10, 3)	-0.00066101	-0.00388223	-0.00114269	-0.00055603
G(10, 4)	0.00008724	0.00074602	-0.00011554	0.00065723
G(10, 5)	0.00025215	-0.00208807	-0.00198654	0.00389784
G(10, 6)	-0.00006693	-0.00000766	-0.00207007	0.00076030
G(10, 7)	0.00000193	-0.00048725	-0.00091080	0.00104582
G(10, 8)	-0.00002157	0.00409447	0.00283651	-0.00236132
G(10, 9)	0.00000006	-0.00000928	0.00000798	-0.00000279
G(10,10)	-0.00000024	-0.00000075	-0.00000099	-0.00000673

	$\alpha=180^o$	$\alpha=225^o$	$\alpha=270^o$	$\alpha=315^o$
G(1, 0)	-0.57709616	-0.60913002	-0.59894407	-0.57591563
G(1, 1)	0.08275084	0.09057575	0.01329215	-0.11578742
G(2, 0)	-0.01108434	0.01270898	-0.00486850	-0.00385498
G(2, 1)	-0.34384710	-0.33929998	-0.33729932	-0.27290040
G(2, 2)	0.04621552	0.04103137	0.01010815	-0.02995886
G(3, 0)	-0.07644648	-0.08444408	-0.07707080	-0.09643058
G(3, 1)	0.04434624	0.05318312	-0.00240211	-0.05514626
G(3, 2)	-0.07423157	-0.07325980	-0.06168517	-0.05059413
G(3, 3)	0.01204483	0.01398113	0.00289209	-0.00256676
G(4, 0)	-0.04176808	-0.02324794	-0.00744605	0.02156326
G(4, 1)	-0.14265783	-0.13486916	-0.13656057	-0.10843159
G(4, 2)	0.03147948	0.04771406	0.00395409	-0.03775156
G(4, 3)	-0.00389880	-0.00056901	0.00208133	0.00200035
G(4, 4)	-0.00167083	0.00795771	0.00314189	-0.00022783
G(5, 0)	-0.01109254	-0.00534653	-0.00540425	-0.01774592
G(5, 1)	0.00625649	0.01327408	-0.00410884	-0.03834093
G(5, 2)	-0.06505450	-0.06661368	-0.08604892	-0.06183620
G(5, 3)	0.00184782	0.03050842	0.00342938	-0.01202911
G(5, 4)	0.00533381	0.00019979	-0.00712004	-0.00147357
G(5, 5)	-0.00208303	0.00299644	0.00240486	-0.00146445
G(6, 0)	-0.03059197	-0.00816103	0.00140552	0.02565001
G(6, 1)	-0.07946639	-0.05232975	-0.05480205	-0.03017620
G(6, 2)	0.01699269	0.02175780	0.00804942	-0.03378105
G(6, 3)	-0.00686086	-0.02262488	-0.03865689	-0.01780634
G(6, 4)	-0.01435987	0.02279052	0.00132799	0.00099575
G(6, 5)	0.00520626	-0.00021826	-0.01197919	-0.00299620
G(6, 6)	-0.00154688	0.00479181	0.00416743	-0.00189914
G(7, 0)	0.01971844	0.01200576	0.01355736	-0.01727920
G(7, 1)	0.00955503	0.00112343	-0.00277094	-0.00150154
G(7, 2)	-0.05982944	-0.02817035	-0.04429442	-0.02856826
G(7, 3)	0.00267487	0.01890461	0.00819583	-0.02007250
G(7, 4)	0.01203409	-0.00290631	-0.00995578	-0.00200535
G(7, 5)	-0.01222808	0.01218658	-0.00085391	0.00432861
G(7, 6)	0.00183056	-0.00523453	-0.00832791	0.00036418

	$\alpha=180^{\circ}$	$\alpha=225^{\circ}$	$\alpha=270^{\circ}$	$\alpha=315^{\circ}$
G(7, 7)	-0.00210364	0.00251089	0.00473227	-0.00330430
G(8, 0)	-0.02000607	-0.00113438	0.00118011	0.00501335
G(8, 1)	-0.00000762	0.00000660	-0.00000005	-0.00008275
G(8, 2)	0.00019176	-0.00007228	0.00000001	0.00002353
G(8, 3)	-0.02702314	-0.01217487	-0.02555243	-0.01238130
G(8, 4)	-0.00447119	0.00616529	0.00269019	-0.00550030
G(8, 5)	0.00695114	0.00245640	-0.00477784	-0.00017510
G(8, 6)	-0.00974452	0.00796753	-0.00120304	0.00479962
G(8, 7)	0.00226276	-0.00239843	-0.00091922	0.00006179
G(8, 8)	-0.00202971	0.00056569	0.00433292	-0.00297690
G(9, 0)	-0.01033668	-0.01000137	-0.00067857	-0.03044157
G(9, 1)	0.00152764	-0.00010562	-0.00048214	-0.00004036
G(9, 2)	-0.00004681	0.00005837	-0.00021124	0.00007267
G(9, 3)	-0.00476104	0.00161330	0.00228422	-0.00166715
G(9, 4)	-0.00464545	-0.00275073	-0.00940238	-0.00413898
G(9, 5)	-0.00280360	0.00289581	-0.00217455	-0.00216732
G(9, 6)	-0.00207030	0.00070886	-0.00249742	-0.00017582
G(9, 7)	-0.00409556	0.00299261	-0.00062696	0.00255423
G(9, 8)	0.00127051	-0.00028279	0.00041439	-0.00059604
G(9, 9)	-0.00326805	0.00052126	0.00333244	-0.00092754
G(10, 0)	-0.00094684	0.00003501	0.00017572	0.00002547
G(10, 1)	-0.00025991	-0.00016511	-0.00009792	-0.00031670
G(10, 2)	0.00112341	-0.00080817	0.00122698	0.00013672
G(10, 3)	-0.00230579	-0.00099702	-0.00252340	-0.00023840
G(10, 4)	-0.00318032	-0.00104373	0.00281916	-0.00048342
G(10, 5)	0.00375016	-0.00009449	-0.00145509	0.00028287
G(10, 6)	-0.00236521	-0.00054373	-0.00085616	-0.00046020
G(10, 7)	-0.00159140	0.00002960	-0.00173427	0.00052795
G(10, 8)	-0.00261024	0.00041239	0.00012128	0.00057350
G(10, 9)	0.00000505	0.00000053	0.00000181	-0.00000112
G(10,10)	-0.00000605	0.00000012	0.00000627	-0.00000064

Appendix B

Functional Representations G(n,m,α) of the Expansion Coefficients of the Associated Legendre Functions Which Represent the Magnetic Potential Due to Magnetopause Surface Currents

$$G(1,0,\alpha) = - (.0403 * Cos(\alpha) - (.98332)*(.38/\pi^2)*Cos(\alpha) - 3.10310*(.32/(9\pi^2))*Cos(3\alpha) - .806*(.32/(25\pi^2))*Cos(5\alpha) - .806*(.4/(49\pi^2))*Cos(7\alpha) + .00702*Cos(2\alpha) + .00494*Cos(4\alpha) - .0172*Sin(.5\alpha) - .5823)$$

$$G(1,1,\alpha) = - (6*(.38/\pi^2*Cos(\alpha) + (.32/(9\pi^2))*Cos(3\alpha) + (.32/(25\pi^2))*Cos(5\alpha) + (.4/(49\pi^2))*Cos(7\alpha)) - .35*Cos(\alpha) - .008*Cos(2\alpha) + .007*Cos(4\alpha) - .0005)$$

$$G(2,0,\alpha) = - (2.475*((.38/(\pi^2))*Cos(\alpha) + (.32/(9\pi^2))*Cos(3\alpha) + (.32/(25\pi^2))*Cos(5\alpha) + (.4/(49\pi^2))*Cos(7\alpha)) - .097*Cos(\alpha) - .0032*Cos(4\alpha) + .003*Cos(2\alpha) - (.1/(25\pi^2))*Cos(5\alpha) + .001)$$

$$G(2,1,\alpha) = - (.0969*Cos(\alpha) + .13357*Sin(.5\alpha) - .855*(.38/\pi^2*Cos(\alpha) + (.32/(9\pi^2))*Cos(3\alpha) + (.32/(25\pi^2))*Cos(5\alpha) + (.4/(49\pi^2))*Cos(7\alpha)) + .00551*Cos(\alpha) - .00285*Cos(4\alpha) - .41)$$

$$G(2,2,\alpha) = - (.3*((.38/\pi^2)*Cos(\alpha) + (.32/(9\pi^2))*Cos(3\alpha) + (.32/(25\pi^2))*Cos(5\alpha) + (.4/(49\pi^2))*Cos(7\alpha)) - .0593*Cos(\alpha) - .0029*Cos(2\alpha) - .00158*Cos(4\alpha) + .0047)$$

$$G(3,0,\alpha) = - (- .03773*Cos(\alpha) - .04921*Sin(.5\alpha) + .287*((.38/\pi^2)*Cos(\alpha) + (.32/(9\pi^2))*Cos(3\alpha) + (.32/(25\pi^2))*Cos(5\alpha) + (.4/(49\pi^2))*Cos(7\alpha)) + .0063*Cos(4\alpha) - .0077*Cos(2\alpha) - .051)$$

$$G(3,1,\alpha) = - (3.1*((.38/\pi^2)*Cos(\alpha) + (.32/(9\pi^2))*Cos(3\alpha) + (.32/(25\pi^2))*Cos(5\alpha) + (.4/(49\pi^2))*Cos(7\alpha)) - .1835*Cos(\alpha) - .0001)$$

G(3,2,α) = − (.05165*Cos(α) + .1*Sin(.5α) − .1325*((.38/π²)*Cos(α) + (.32/(9π²))*Cos(3α) + (.32/(25π²))*Cos(5α) + (.4/(49π²))*Cos(7α)) + .0029*Cos(α) + .0013*Cos(4α) − .1268)

G(3,3,α) = − (− .3096*((.32/π²)*Cos(α) + (.32/(9π²))*Cos(3α) + (.32/(25π²))*Cos(5α) + (.32/(49π²))*Cos(7α)) + .001)

G(4,0,α) = − (.9625*((.38/π²)*Cos(α) + (.32/(9π²))*Cos(3) + (.32/(25π²))*Cos(5α) − (.2/(49π²))*Cos(7α) + (.6/(16π²))*Cos(2α) − (.24/(16π²))*Cos(4α)) − .00225)

G(4,1,α) = − (.024012*Cos(α) + .046*Sin(.5α) − .00276*Cos(2α) − .00092*Cos(4α) − .16074)

G(4,2,α) = − (3.415*((.38/π²)*Cos(α) + (.32/(9π²))*Cos(3α) + (.32/(25π²))*Cos(5α) + (.4/(49π²))*Cos(7α)) − .181*Cos(α) − .002*Cos(2α) + .0025)

G(4,3,α) = − (.8*(− .005*Cos(2α) + .00122*Cos(α) + .001*Cos(4α)) + .0003)

G(4,4,α) = − (.65*(.56*((.38/π²)*Cos(α) + (.7/(9π²))*Cos(3α) + (.32/(25π²))*Cos(5α) + (.4/(49π²))*Cos(7α)) − .0261*Cos(α) − .003*Cos(2α)) + .001)

G(5,0,α) = − (.0025*Cos(3α) + .00084*Cos(α) − .00072*Cos(2α) + .0001*Cos(4α) − .00715)

G(5,1,α) = − (.5*(1.6*((.38/π²)*Cos(α) + (.95/(9π²))*Cos(3α) + (.32/(25π²))*Cos(5α) + (.4/(49π²))*Cos(7α)) − .0985*Cos(α) + .004*Cos(4α) + .002*Cos(2α)) − .005)

$G(5,2,\alpha) = - (.006*Cos(3\alpha) + .008*Cos(2\alpha) - .0034*Cos(\alpha) - .002*Cos(4\alpha) - .001*Cos(5\alpha) - .0695)$

$G(5,3,\alpha) = - (.6*(- .0303*Cos(\alpha) + .03*Cos(3\alpha) - .006*Cos(4\alpha)) + .0052)$

$G(5,4,\alpha) = - (- .00296*Cos(\alpha) + .0033*Cos(2\alpha) + .001*Cos(4\alpha) - .0019)$

$G(5,5,\alpha) = - (.77*(- .0022*Cos(\alpha) + .0042*Cos(3\alpha) - .003*Cos(2\alpha) + .0006*Cos(4\alpha)) + .0013)$

$G(6,0,\alpha) = - (((.279248671/\pi^2)*Cos(\alpha) - .0002868*Cos(2\alpha) + (.02936985/(9\pi^2))*Cos(3\alpha) - .00346*Cos(4\alpha) + (.193610650/(25\pi^2))*Cos(5\alpha) + (.193610650/49\pi^2))*Cos(7\alpha) + .003016240)$

$G(6,1,\alpha) = - (.0082*Cos(\alpha) - .0103*Cos(2\alpha) - .0092*Cos(4\alpha) - .0517)$

$G(6,2,\alpha) = - (- .028*Cos(\alpha) - .0035*Cos(2\alpha) + .0072*Cos(3\alpha) + .0015*Cos(4\alpha) - .0018)$

$G(6,3,\alpha) = - (.003*Cos(\alpha) + .017*Cos(2\alpha) + .0017*Cos(4\alpha) - .0225)$

$G(6,4,\alpha) = - (.72*(- .0058*Cos(\alpha) - .0051*Cos(2\alpha) + .015*Cos(3\alpha) - .007*Cos(4\alpha)) + .001)$

$G(6,5,\alpha) = - (.485*(- .0037*Cos(\alpha) + .013*Cos(2\alpha) - .0075*Cos(3\alpha)) - .0065)$

$G(6,6,\alpha) = - (.81*(- .00235*Cos(\alpha) - .0022*Cos(2\alpha) + .004*Cos(3\alpha) - .00032*Cos(4\alpha)) + .00181)$

$G(7,0,\alpha) = - (.72*(- .007*Cos(\alpha) + .005*Cos(2\alpha) + .009*Cos(3\alpha) + .015*Cos(4\alpha)) + .007)$

$G(7,1,\alpha) = - (.92*(.0041*Cos(\alpha) + .01*Cos(2\alpha) + .0036*Cos(4\alpha)) + .0007)$

$G(7,2,\alpha) = -(1.03*(.0022*Cos(\alpha) - .0075*Cos(2\alpha) + .0034*Cos(3\alpha) - .01*Cos(4\alpha)) - .036)$

$G(7,3,\alpha) = -(.83*(-.0204*Cos(\alpha) - .001*Cos(2\alpha) + .017*Cos(3\alpha) - .0027*Cos(4\alpha)) + .0032)$

$G(7,4,\alpha) = -(.955*(-.0024*Cos(\alpha) + .012*Cos(2\alpha) + .0012*Cos(3\alpha) + .0007*Cos(4\alpha)) - .00135)$

$G(7,5,\alpha) = -(.815*(-.0013*Cos(\alpha) - .0041*Cos(2\alpha) + .006*Cos(3\alpha) - .0078*Cos(4\alpha)) + .0013)$

$G(7,6,\alpha) = -(.94*(.0042*Cos(\alpha) + .0044*Cos(2\alpha) - .006*Cos(3\alpha) + .0025*Cos(4\alpha)) - .0063)$

$G(7,7,\alpha) = -(.6*(-.00335*Cos(\alpha) - .001*Cos(2\alpha) + .005*Cos(3\alpha) - .0015*Cos(4\alpha)) + .00035)$

$G(8,0,\alpha) = -(.92*(.0065*Cos(\alpha) - .008*Cos(2\alpha) + .0032*Cos(3\alpha) - .0032*Cos(4\alpha)) - .0008)$

$G(8,1,\alpha) = -(.9*(.000013*Cos(\alpha) + .00005*Cos(3\alpha) + .00008*Cos(4\alpha)) - .0000237)$

$G(8,2,\alpha) = -(.6*(-.00005*Cos(\alpha) + .0001*Cos(2\alpha) - .00012*Cos(3\alpha) + .000075*Cos(4\alpha)) - .000015)$

$G(8,3,\alpha) = -(.665*(.005*Cos(\alpha) - .0005*Cos(2\alpha) + .003*Cos(3\alpha) - .0035*Cos(4\alpha)) - .019)$

$G(8,4,\alpha) = -(-.00207*Cos(\alpha) - .00105*Cos(2\alpha) + .005*Cos(3\alpha) - .0006*Cos(4\alpha) + .00012)$

$G(8,5,\alpha) = -(.88*(-.0019*Cos(\alpha) + .005*Cos(2\alpha) - .0019*Cos(3\alpha)) - .00085)$

$G(8,6,\alpha) = -(.9*(.0022*Cos(\alpha) - .004*Cos(2\alpha) + .0022*Cos(3\alpha) - .003*Cos(4\alpha)) + .0005)$

$G(8,7,\alpha) = - (.8*(.0036*Cos(\alpha) + .001*Cos(2\alpha) - .005*Cos(3\alpha) + .004*Cos(4\alpha)) - .00288)$

$G(8,8,\alpha) = - (- .0006*Cos(\alpha) - .0009*Cos(2\alpha) + .0014*Cos(3\alpha) + .0005*Cos(4\alpha) - .00085)$

$G(9,0,\alpha) = - (1.1*(- .0022*Cos(\alpha) - .002*Cos(2\alpha) + .0137*Cos(3\alpha) + .015*Cos(4\alpha)) - .012)$

$G(9,1,\alpha) = - (1.33*(- .0001*Cos(\alpha) + .00033*Cos(2\alpha) - .0005*Cos(3\alpha) + .0002*Cos(4\alpha)) + .00003)$

$G(9,2,\alpha) = - (1.05*(- .00016*Cos(\alpha) + .00024*Cos(2\alpha) + .00006*Cos(3\alpha) - .00035*Cos(4\alpha)) - .00002)$

$G(9,3,\alpha) = - (.95*(- .00285*Cos(\alpha) - .0037*Cos(2\alpha) + .005*Cos(3\alpha) - .0003*Cos(4\alpha)) + .0010575)$

$G(9,4,\alpha) = - (.75*(- .0026*Cos(\alpha) + .0058*Cos(2\alpha) + .005*Cos(3\alpha) - .0032*Cos(4\alpha)) - .0048)$

$G(9,5,\alpha) = - (.91*(- .0024*Cos(\alpha) + .0009*Cos(2\alpha) + .004*Cos(3\alpha) - .0022*Cos(4\alpha)) - .00008)$

$G(9,6,\alpha) = - (.7*(.000515*Cos(\alpha) + .00071*Cos(2\alpha) + .0006*Cos(3\alpha) - .00032*Cos(4\alpha)) - .00158)$

$G(9,7,\alpha) = - (1.05*(.00154*Cos(\alpha) - .0018*Cos(2\alpha) + .0003*Cos(3\alpha) - .0011*Cos(4\alpha)) + .00085)$

$G(9,8,\alpha) = - (1.64*(.00061*Cos(\alpha) + .00001*Cos(2\alpha) - .001*Cos(3\alpha) + .0008*Cos(4\alpha)) - .00069)$

$G(9,9,\alpha) = - (1.13*(.001*Cos(\alpha) - .00145*Cos(2\alpha) + .0003*Cos(3\alpha) + .00055*Cos(4\alpha)) - .00077)$

$G(10,0,\alpha) = - (.7*(.00019*Cos(\alpha) - .0004*Cos(2\alpha) + .0005*Cos(3\alpha) - .00026*Cos(4\alpha)) + .000002)$

$G(10,1,\alpha) = -(.55*(-.00004*Cos(\alpha) - .00024*Cos(2\alpha) + .0004*Cos(3\alpha) + .0005*Cos(4\alpha)) - .00021)$

$G(10,2,\alpha) = -(.88*(-.0002*Cos(\alpha) + .00012*Cos(2\alpha) - .0005*Cos(3\alpha) + .0003*Cos(4\alpha)) + .00012)$

$G(10,3,\alpha) = -(.00018*Cos(2\alpha) + .00083*Cos(3\alpha) - .0001*Cos(4\alpha) - .00157)$

$G(10,4,\alpha) = -(1.16*(.0008*Cos(\alpha) - .00125*Cos(2\alpha) + .0006*Cos(3\alpha) - .00002*Cos(4\alpha)) - .00007)$

$G(10,5,\alpha) = -(-.00185*Cos(\alpha) + .00185*Cos(2\alpha) + .0001*Cos(3\alpha) - .0002*Cos(4\alpha) + .00034)$

$G(10,6,\alpha) = -(.00045*Cos(\alpha) + .00013*Cos(2\alpha) + .0007*Cos(3\alpha) - .00063*Cos(4\alpha) - .00071)$

$G(10,7,\alpha) = -(.00022*Cos(\alpha) + .00026*Cos(2\alpha) + .00058*Cos(3\alpha) - .00067*Cos(4\alpha) - .00039)$

$G(10,8,\alpha) = -(.0018*Cos(\alpha) - .0014*Cos(2\alpha) - .0005*Cos(3\alpha) - .0003*Cos(4\alpha) + .0004)$

$G(10,9,\alpha) = -(1.04*(-.0000026*Cos(\alpha) - .0000011*Cos(2\alpha) + .0000002*Cos(3\alpha) + .0000033*Cos(4\alpha)) + .0000000208)$

$G(10,10,\alpha) = -(.96*(.0000025*Cos(\alpha) - .000003*Cos(2\alpha) + .0000005*Cos(3\alpha) + .0000009*Cos(4\alpha)) - .00000115)$